ARCTIC
VOL. 49, NO. 4 (DECEMBER 1996) P. 367–374

A Method To Determine Lake Depth and Water Availability on the North Slope of Alaska with Spaceborne Imaging Radar and Numerical Ice Growth Modelling

M.O. JEFFRIES,[1] K. MORRIS[1] and G.E. LISTON[2]

(*Received 21 December 1995; accepted in revised form 27 June 1996*)

ABSTRACT. Spaceborne synthetic aperture radar (SAR) images and numerical ice growth modelling were used to determine maximum water depth and water availability in two areas of the North Slope in northwestern Alaska. SAR images obtained between September 1991 and May 1992 were used to identify when and how many lakes froze completely to the bottom, and how many lakes did not freeze completely to the bottom. At Barrow, on the coast, 60% of the lakes froze completely to the bottom in mid-January alone, and by the end of winter 77% of the lakes were completely frozen. In contrast, 100 km to the south in the 'B' Lakes region, only 23% of the lakes froze completely, and there was no sudden freezing of many lakes as occurred at Barrow. A physically based, numerical model was used to simulate ice growth on the lakes. The simulated maximum ice thickness is 2.2 m. Consequently, any lake where some part of the ice cover does not freeze to the bottom has some water more than 2.2 m deep. For those lakes where the ice cover had frozen completely at some time in the winter, the simulated ice growth curve provides the ice thickness at the time each lake had frozen completely to the bottom and thus the lake's maximum water depth. At Barrow, 60% of the lakes are between 1.4 m and 1.5 m deep, and 23% are more than 2.2 m deep. At the 'B' Lakes, 77% of the lakes are more than 2.2 m deep. Thus, there is a considerable contrast in lake depth and water availability between the Barrow and the 'B' Lakes regions. This method is simple to implement, and the relatively inexpensive SAR data have good spatial and temporal coverage. This method could be used to determine lake depth and water availability on the entire North Slope and in other polar and subpolar areas where shallow lakes are common.

Key words: Synthetic Aperture Radar, Alaskan North Slope, lake ice, lake depth, water availability.

RÉSUMÉ. On s'est servi d'images prises au radar à antenne latérale synthétique (RALS) spatioporté et d'une modélisation numérique de la formation de la glace pour déterminer la profondeur d'eau maximale et la disponibilité de cette eau dans deux régions du versant Nord dans le nord-est de l'Alaska. Des images RALS obtenues entre septembre 1991 et mai 1992 ont servi à identifier quand et comment un grand nombre de lacs avaient gelé sur toute leur profondeur et comment cela ne s'était pas produit pour bien d'autres. À Barrow, sur la côte, 60 p. cent des lacs avaient déjà gelé sur toute leur profondeur à la mi-janvier et, à la fin de l'hiver, 77 p. cent des lacs avaient complètement gelé. Par contre, à 100 km plus au sud, dans la région des lacs "B", seulement 23 p. cent des lacs avaient complètement gelé, et on n'observait pas l'engel soudain de nombreux lacs comme c'était le cas à Barrow. On s'est servi d'un modèle numérique fondé sur des critères physiques pour simuler la formation de la glace sur les lacs. L'épaisseur maximale de la glace simulée est de 2,2 m. En conséquence, tout lac où une partie du manteau glaciel n'atteint pas le fond a une profondeur supérieure à 2,2 m. Pour les lacs dont le manteau glaciel atteignait le fond à un moment quelconque de l'hiver, la courbe de formation simulée de la glace donne l'épaisseur de la glace au moment où chaque lac a gelé sur toute sa profondeur, et donc, la profondeur maximale de ce lac. À Barrow, 60 p. cent des lacs ont entre 1,4 et 1,5 m de profondeur et 23 p. cent ont plus de 2,2 m de profondeur. Dans la région des lacs "B", 77 p. cent des lacs ont plus de 2,2 m de profondeur. Il y a donc un fort contraste dans la profondeur des lacs et la disponibilité de l'eau entre la région de Barrow et celle des lacs "B". Cette méthode est facile à appliquer et les données RALS — relativement bon marché — offrent une bonne couverture spatiale et temporelle. On pourrait utiliser cette méthode pour déterminer la profondeur des lacs et la disponibilité de l'eau sur tout le versant Nord et dans d'autres zones polaires et subpolaires où se trouve un grand nombre de lacs peu profonds.

Mots clés: radar à antenne latérale synthétique, versant Nord de l'Alaska, glace lacustre, profondeur de lac, disponibilité de l'eau

Traduit pour la revue *Arctic* par Nésida Loyer.

INTRODUCTION

Shallow thaw lakes are a major component of the tundra landscape of the Alaskan North Slope, where they comprise over 20% of the total area and perhaps as much as 40% of the area of the Coastal Plain (Sellmann et al., 1975a). All or part of most lakes are less than 2 m deep; consequently, a significant area of water freezes completely to the bottom each winter (Sellmann et al., 1975a; Mellor, 1982). There are only a few weeks each year when the lakes are completely ice-free.

[1] Geophysical Institute, University of Alaska Fairbanks, 903 Koyukuk Drive, P.O. Box 757320, Fairbanks, Alaska 99775-7320, U.S.A.
[2] Department of Atmospheric Science, Colorado State University, Fort Collins, Colorado 80523, U.S.A.

The lake depth and ice growth and decay determine the value of the lakes as habitats for wildlife and aquatic fauna and their usefulness as sources of fresh water for settlements and industrial development (Sellmann et al., 1975a; Mellor, 1982, 1994). While it is known that few lakes exceed 2 m in depth, the bathymetry of most lakes is unknown, and the geographic variability of lake depth in different watersheds is poorly mapped. More precise information of this kind would help to define natural resource values; develop, manage, and enhance water resources; and mitigate the effects of potentially conflicting uses (Mellor, 1994).

Our method combined spaceborne remote sensing and numerical ice growth modelling to determine lake depth and water availability in two regions of the North Slope in northwestern Alaska. We used synthetic aperture radar (SAR) to determine where lake ice was frozen completely to the lake bottom and where it still had liquid water below it. SAR-derived data show when and how many lakes freeze completely to the bottom in each region. A numerical ice growth model was used to determine the ice thickness at the time each lake freezes completely to the bottom and thus maximum lake depth. We present data on lake depth variability in each region.

STUDY AREAS, ENVIRONMENTAL DATA SOURCES, AND SAR DATA

The period of the study was September 1991 to May 1992. The first study area, the Barrow Lakes, is located in the vicinity of Pt. Barrow (Fig. 1), where the lakes are located close to the coast at elevations near sea level. The second study area, the 'B' Lakes, is located 100 km south of Pt. Barrow at an elevation of about 35 m above sea level. Mellor (1982) referred to this as "Area B" in his study of lake ice remote sensing. In general, the 'B' Lakes are greater in number and smaller in size, and have a more dense areal coverage than those in the Barrow region (Fig. 2). The ice growth and decay history at the Barrow lakes and at the 'B' Lakes is similar each year; i.e., the timing of freeze-up and initial ice formation in autumn and the onset of melt in spring coincide (Morris et al., 1995).

A National Weather Service station at Barrow was the source of air temperature, precipitation, and wind speed and direction data for inputs to the ice growth model that we used to simulate lake ice growth in both study areas. No weather data are available for the 'B' Lakes, and the use of Barrow weather data to represent the 'B' Lakes was considered reasonable in view of the concordance of the ice growth and decay histories for each area. In addition, snow and ice thickness data that were obtained in April 1992 at a number of Barrow lakes (Jeffries et al., 1994) were used for running and validating the ice growth model.

The SAR images were obtained from the Alaska SAR Facility (ASF), a station operated by the University of Alaska Fairbanks under contract to NASA for the reception and processing of raw radar signal data into image form. For this study, we used images produced with data from the C-band (5.3 GHz frequency, 57 mm wavelength) SAR aboard the European Space Agency (ESA) ERS-1 satellite. The images are ASF Standard Low Resolution products. They comprise 1024 lines, each containing 1024 pixels, with 100 m pixel size and 240 m resolution. A full SAR image has ground dimensions of 100 km by 100 km.

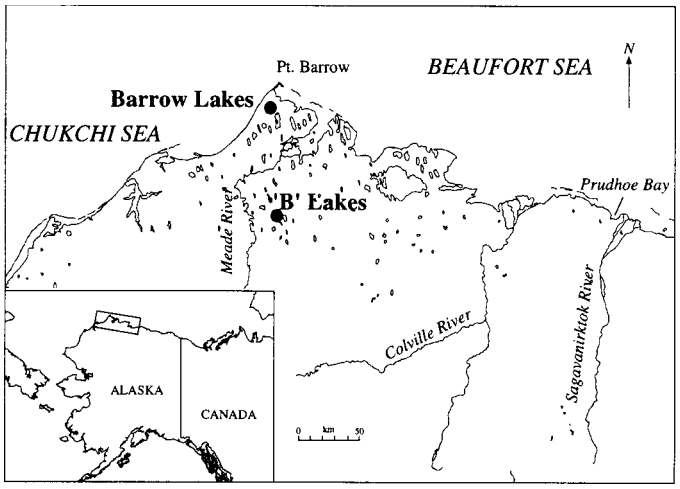

FIG. 1. Map of the study area showing the location of the Barrow and 'B' Lakes regions in northwestern Alaska.

SAR REMOTE SENSING OF LAKE ICE GROWTH AND BOTTOM FREEZING

Background

In the SAR image (Fig. 2), the lakes are characterized by a variety of dark and light tones; some lakes are completely dark, while others have a combination of dark tones around the margin and light tones in the centre. The proportion of light and dark tones in individual lakes changes during the course of the winter (Fig. 3). The area of dark tone increases from the margins towards the centres of lakes, and while an area of bright tone might remain in the centre of some lakes all winter (Lakes I and II, Fig. 3), other lakes become completely dark (Lakes III and IV, Fig. 3).

The grey tones in the SAR images are a visual measure of the strength of the radar backscatter from the ice, which is determined by the presence of tubular air inclusions in the ice and whether the ice has liquid water at the base or is frozen to the bottom of the lake (Sellmann et al., 1975b; Elachi et al., 1976; Weeks et al., 1977, 1978, 1981; Jeffries et al., 1994; Wakabayashi et al., 1994). The light tones denote strong backscatter from ice that has liquid water beneath it. Here, backscatter is strong because of the combined effects of reflection off the ice–water interface, which has a strong dielectric contrast, and forward scattering off the tubular bubbles. The dark tones denote low backscatter from ice that is frozen to the bottom of the lake. Here, the weak dielectric contrast between the ice and frozen soil of the lake bed allows the radar signal to pass into the soil, where it is absorbed.

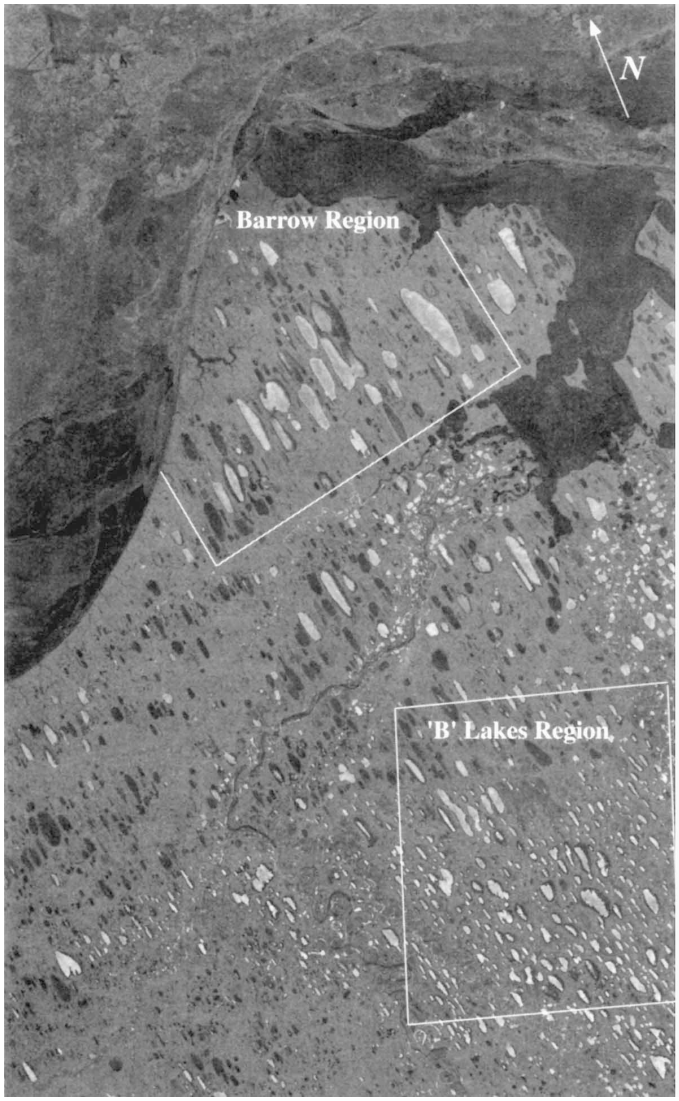

FIG. 2. A mosaic of two ERS-1 SAR images of a 100 km by 200 km area of northwestern Alaska on 2 March 1992, showing the location of the Barrow and 'B' Lakes study areas. Note the spatial variation in the density of lakes and the variability of the grey tones of the lake ice. The long axes of most of the lakes have a preferred orientation in a nearly north-south direction, perpendicular to the prevailing winds that promote wave and current erosion primarily at the ends of the lakes (Carson and Hussey, 1962). SAR image copyright rests with ESA.

In Figure 2, then, it is apparent that the entire lake ice cover on many lakes had frozen completely to the bottom by early March. At other lakes at that time, there remained a significant area of ice with liquid water at the base. The gradual increase in area of dark tones from the margins of lakes towards their centres (Fig. 3) reflects their bathymetry. The margins are shallower than the centres, and as the winter progresses and the ice thickens, it first freezes to the bottom around the perimeter and then freezes progressively inwards towards the centre. If some part of a lake is deep enough to exceed the maximum possible annual ice thickness, liquid water will remain below the ice at the end of winter (Lakes I and II, Fig. 3), but if the deepest water is shallower than the maximum ice thickness, then the entire area of lake ice will freeze completely to the bottom (Lakes III and IV, Fig. 3).

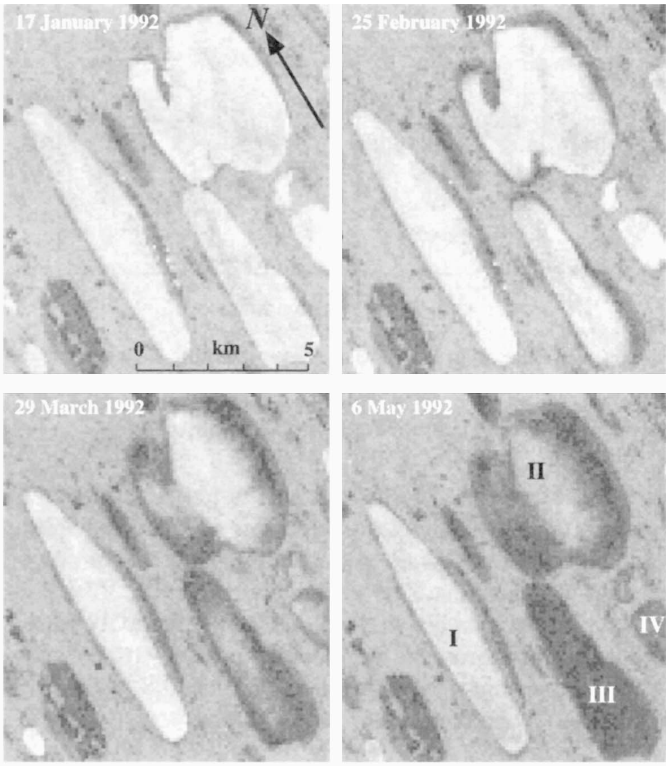

FIG. 3. ERS-1 SAR subscenes of lakes in the Barrow region illustrate spatial changes in tone (i.e., backscatter intensity) due to the progressive freezing of ice to all or part of the bottom of the lakes between January and May 1992. Bright tones are areas of ice where there is water between the ice and the lake bottom. Dark tones are areas of ice that are frozen to the lake bottom. Lakes I, II, III, and IV are referred to in the text. Copyright of the SAR images rests with ESA.

The timing of complete freezing will depend on the maximum water depth.

Timing and Number of Lakes Freezing to the Bottom

For this study, a time series of SAR images from the onset of ice growth in early September 1991 until the onset of melt in May 1992 was assembled for each region, 32 images for the Barrow region and 18 for the 'B' Lakes region. The difference in image numbers reflects the data acquisition schedule, which is controlled by ESA, and the resultant frequency of data transmission to ASF. The backscatter or tonal changes of the ice on 180 lakes in the Barrow region and 293 lakes in the 'B' region were monitored during the course of the winter. The difference in lake numbers reflects the greater number of lakes in the 'B' Lakes region (Fig. 2). With the aid of the SAR image time series, we noted the date when the tone of a lake went completely dark, indicating that the entire area of lake ice had frozen to the bottom. In this way, records were compiled of the dates on which individual lakes froze completely and of the number of lakes that did and did not freeze completely to the bottom.

The results of the SAR image analysis are summarized in Figure 4. In both regions, lakes began to freeze completely to the bottom in mid-to-late November. By the end of winter, 68 lakes in the 'B' Lakes region (23% of the total) and 139 lakes

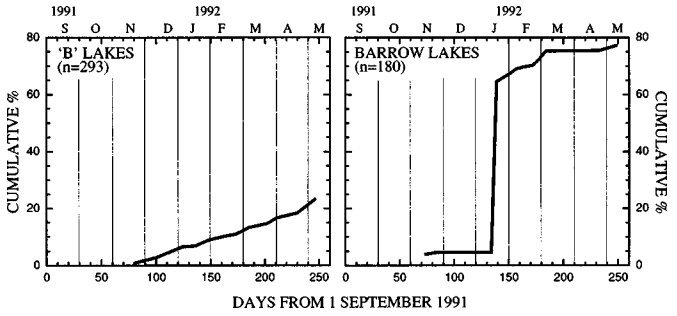

FIG. 4. Graphs illustrating the number of lakes that froze completely to the bottom, and when that occurred in winter 1991–92 in the 'B' Lakes and Barrow regions. The number of lakes (*y* axis) is given as a cumulative percentage of the total number of lakes (n) that were monitored during the winter.

in the Barrow region (77% of the total) had frozen completely to the bottom. Not only did the number of lakes that freeze completely differ in each region, but the pattern of timing of freezing was different. The freezing curve for the 'B' Lakes shows a steady increase in the number of completely frozen lakes, while at Barrow the number of completely frozen lakes remained constant until mid-January, when 108 lakes (60% of the total) froze completely to the bottom.

NUMERICAL ICE GROWTH MODELLING

Model Description

When and how many lakes had frozen completely to the bottom was determined from SAR images. The time scale in Figure 4 was converted into ice thickness using a physically based, one-dimensional, nonsteady, numerical model to simulate lake ice growth and thickness. For the lakes that froze completely to the bottom, the ice thickness represents the maximum water depth. Lakes that did not freeze completely to the bottom had some water deeper than the maximum possible ice thickness for winter 1991–92. The maximum possible ice thickness was determined using the numerical ice growth model.

The numerical ice growth model is composed of four major submodels, which are all connected (Liston and Hall, 1995a, 1995b). They can be described briefly as follows. First, a *lake-mixing, energy transport submodel* describes the evolution of lake water temperature and stratification; ice growth is initiated when the upper lake water temperature falls below freezing. Second, a *snow submodel* describes the depth and density of snow as it accumulates, metamorphoses, and melts on top of the lake ice. Third, a *lake ice growth submodel* produces ice by two mechanisms: (1) congelation ice grows at the ice–water interface because energy is transferred from the base to the surface of the ice; and (2) snow ice forms at the lake ice surface from the freezing of water-saturated snow or slush. Fourth, a *surface energy balance submodel* is implemented to determine the surface temperature and energy available for freezing or melting.

The model is governed by the following key equations. The equation describing the one-dimensional temperature distribution and evolution within an ice cover is given by

$$\rho_i C_i \frac{\partial T}{\partial t} = \frac{\partial}{\partial z}\left(k_i \frac{\partial T}{\partial z} \right) + \phi_s(z,t), \qquad (1)$$

where t is time, T is temperature, z is distance measured downward from the top surface, k_i is the ice thermal conductivity, ρ_i is the ice density, C_i is the specific heat of ice, and $\phi_s(z,t)$ is the rate of internal heating of the ice cover due to the absorption of penetrated shortwave radiation.

The boundary condition at the top surface is given by performing a complete surface energy balance of the form

$$(1-\alpha_s)Q_{si} + Q_{li} + Q_{le} + Q_h + Q_e + Q_c = Q_m, \qquad (2)$$

where Q_{si} is the solar radiation reaching the surface, Q_{li} is the incoming longwave radiation, Q_{le} is the emitted longwave radiation, Q_h is the turbulent exchange of sensible heat, Q_e is the turbulent exchange of latent heat, Q_c is the energy transport due to conduction, Q_m is the energy flux available for melt, and α_s is the surface albedo. Each term in Equation (2) is described by an appropriate equation, group of equations, and/or observations. The resulting collection of equations is solved for the surface temperature using the Newton–Raphson iterative solution scheme.

The lower boundary condition at the ice–water interface comprises the balance between the latent heat due to freezing and melting, the energy conducted through the ice, and the heat flux due to convection occurring within the water:

$$\rho_i L \frac{dh}{dt} = k_i \frac{\partial T}{\partial z} - \phi_{wi}(t), \text{ at } z = h \qquad (3)$$

where L is the latent heat of fusion, h is the thickness of the ice cover, and $\phi_{wi}(t)$ is the net heat flux from the water to the ice cover.

The surface energy balance is driven, at a minimum, by observed inputs of minimum and maximum daily air temperatures, wind speed, and precipitation. In addition, the model is capable of taking advantage of observed humidity and radiation components. When the surface energy balance is coupled to the lake-mixing, lake ice, and snow submodels, it provides the surface temperature boundary condition that forces lake water temperatures, lake ice growth, and snow accumulation and metamorphism. In addition to complete energy balance components over the annual cycle, the key outputs are: 1) the time of initial ice formation; 2) time-dependent ice thickness; 3) maximum ice thickness; and 4) time of complete removal of the ice cover.

Model Results

Meteorological data from the National Weather Service station at Barrow were used as inputs to the model. The results of running the model for the Barrow and 'B' Lakes are shown in Figure 5. Three ice growth and decay curves represent different approaches to running the model and dealing with

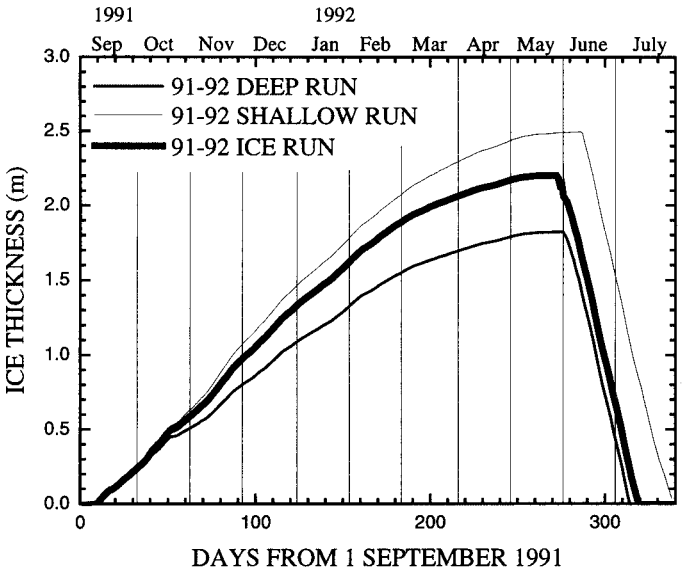

FIG. 5. Simulated lake ice thickness curves illustrate ice growth and decay on the Barrow and 'B' Lakes under three different scenarios. The Deep and Shallow Runs are the results of varying the snow depth input to the numerical ice growth model. The Ice Run is the result of prescribing an ice thickness of 2.15 m as measured in late April 1992 at a number of Barrow lakes where there was water below the ice.

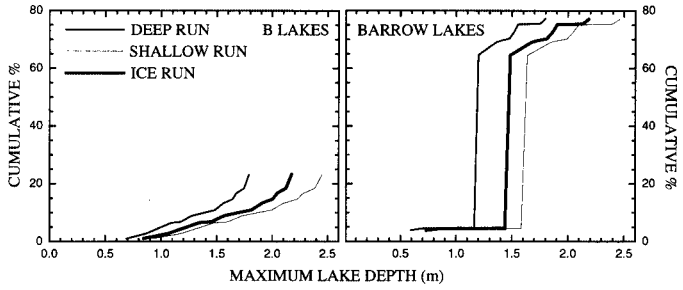

FIG. 6. Graphs illustrating the maximum depth of lakes in the Barrow and 'B' Lakes regions according to the three different ice growth model runs. The number of lakes (*y* axis) with a particular depth is given as a cumulative percentage of the total number of lakes that were monitored during the winter.

uncertainties in the precipitation input. The latter arise because snow accumulation measurements are notoriously difficult to make and generally underestimate the true precipitation totals on the North Slope (Benson, 1982). The precipitation problem was handled by using two extreme precipitation scenarios corresponding to a deep and a shallow snow accumulation. Measurements made in late April 1992 indicated that snow depth on the lakes typically varied between 5 cm and 25 cm. Running the lake ice model in a "data assimilation" mode allows the model to include these snow depth data, so that the precipitation input during the model run leads to a snow depth on the lakes that is equal to the measured snow depth on the observation date. For the case of the 5 cm and 25 cm snow depths, the modelled ice thickness differed by +35 and –25 cm, respectively, from the measured mean thickness (2.15 m) of ice that still had liquid water at its base in late April 1992.

As an alternative, the model was run using the same type of data assimilation procedure, but this time assimilating the ice thickness observations instead of the snow depth data. Thus, the precipitation input during the model run was scaled so that the model produced a snow depth that corresponded to the ice thickness of 2.15 m that was observed in late April 1992. In this run, the snow depth on the lake was 0.13 m. Because the ice depth observations are consistently less variable than the snow depth observations, we believe that the Ice Run provides an ice growth curve that is more representative of the mean ice conditions than the curves produced by the Deep and Shallow snow depth integrations.

Lake Depth Variability

The results of the ice growth model (Fig. 5) allow us to convert the time scale in Figure 4 into a maximum lake depth scale (Fig. 6). Lake depth curves for the Deep, Shallow, and Ice Runs are shown, but we consider only the Ice Run curve. The results can be summarized as follows:

In the 'B' Lakes region,
77% of the lakes are more than 2.2 m deep.

In the Barrow lakes region,
23% of the lakes are more than 2.2 m deep,
10% of the lakes are between 1.5 m and 2.2 m deep,
60% of the lakes are between 1.4 m and 1.5 m deep, and
7% of the lakes are less than 1.4 m deep.

DISCUSSION AND CONCLUSION

We have described for the first time a method that combines spaceborne remote sensing with numerical ice growth modelling to improve our knowledge of the variability of lake depth and water availability on the Alaskan North Slope, where few or no such data were previously available. Winter SAR data of this region clearly identify those lakes where the entire volume of water freezes completely to the bottom, and those lakes where some water remains below the ice at the end of winter. A numerical model is used to simulate lake ice growth and to determine the maximum ice thickness (2.2 m in winter 1991–92). Any lake that freezes completely prior to the time of maximum ice thickness is less than 2.2 m deep, while any lake where water remains below the ice at the time of maximum ice thickness has a maximum water depth greater than 2.2 m. The lakes with a maximum water depth less than 2.2 m freeze completely at different times and the numerical ice growth model, which converts time into ice thickness, contributes to the determination of how many lakes occur in a particular maximum water depth category. The results clearly show that there is significant spatial variability in water depth and availability on the North Slope in northwestern Alaska. That is, in the inland 'B' Lakes region, the lakes are deeper; therefore, far fewer lakes freeze completely to the bottom, and there is greater winter water availability than in the coastal Barrow lakes region.

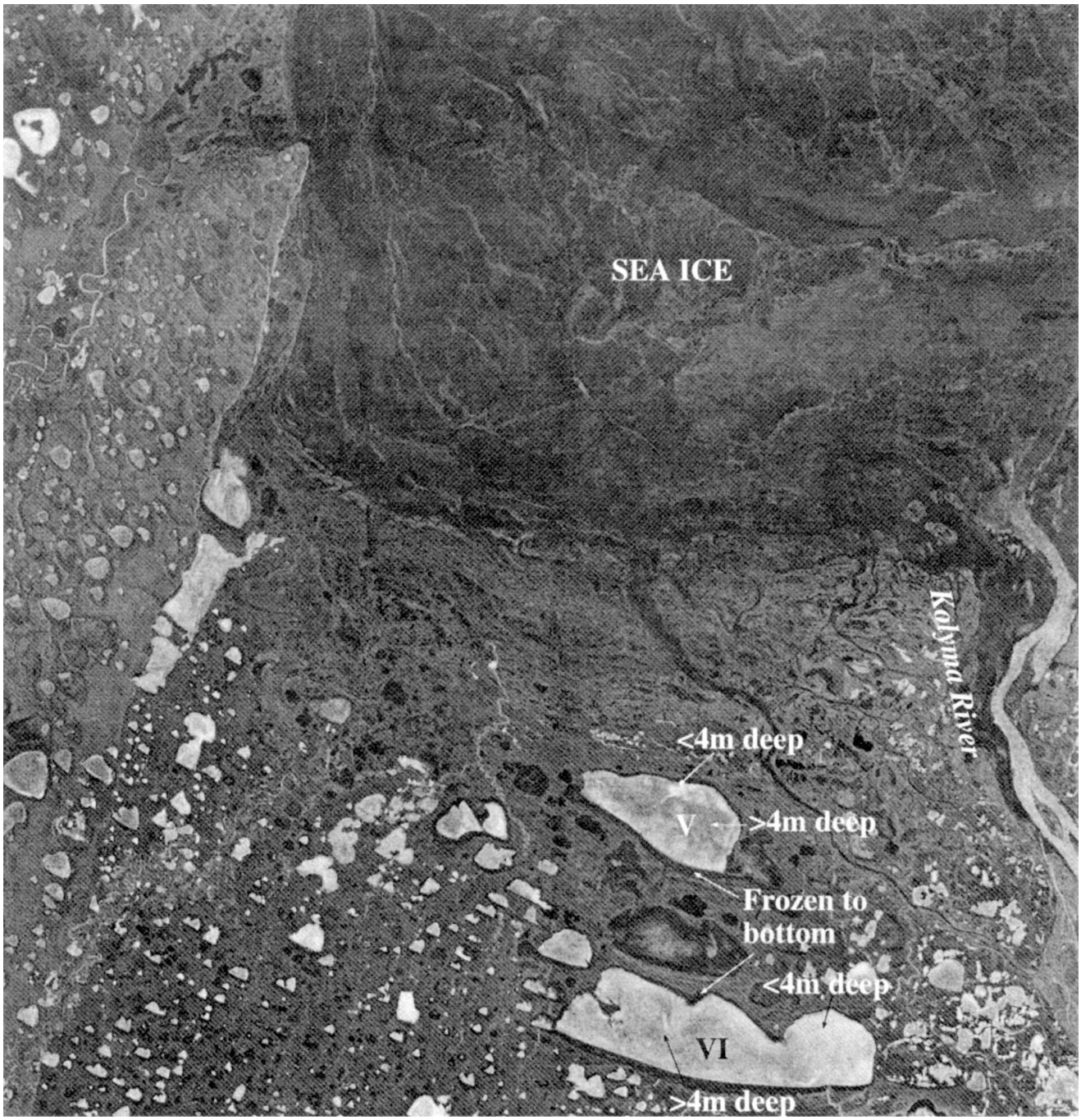

FIG. 7. ERS-1 SAR image of a 100 km × 100 km area immediately to the west of the mouth of the Kolyma River in eastern Siberia on 1 March 1992. The scene centre is at 69.7°N, 160.1°E. There are many lakes in this region and the similarity between their tonal variations and those in northwestern Alaska (Figs. 2 and 3) suggests that they too are shallow. Those areas of Lakes V and VI that, on the basis of backscatter or grey tone variability, are (1) frozen to the bottom, (2) less than 4 m deep, and (3) more than 4 m deep are indicated (after Mellor, 1994). SAR image copyright rests with ESA.

The variability of lake depth and water availability in this small area of the North Slope suggests that there might be similar variability throughout the entire region. This combined remote sensing and numerical ice growth modelling technique is simple to implement, and the SAR data are sufficiently inexpensive and provide extensive geographic coverage; thus, the method could be applied to the entire North Slope and elsewhere. Shallow thaw lakes are widespread in other regions of the Arctic, e.g., (1) the Yukon–Kuskokwim Delta (Morris et al., 1995), (2) northern Yukon Territory, including the Mackenzie River Delta, and the adjacent Northwest Territories; and (3) eastern Siberia (Mellor, 1994).

An ERS-1 SAR image of a small area of eastern Siberia near the Kolyma River delta in late winter 1992 (Fig. 7) shows that the variations in tone (i.e., backscatter variability) of the lakes are similar to those in northwestern Alaska (Figs. 2 and 3). Many of the Siberian lakes are frozen

completely to the bottom, while others still contain water below the ice. The Kolyma River and other rivers to the west also have bright and dark tones that probably indicate those channels that are completely frozen and those that still have water flowing below the ice. In the case of the Kolyma River, there appears to be a single channel, 1.1–2.2 km wide, in which water is flowing out under the sea ice and onto the continental shelf.

Ever since the first airborne radar images of lake ice on the Alaskan North Slope were acquired in the early 1970s, it has been known that the radar signatures were related to lake water depth variability (Sellmann et al., 1975b; Elachi et al., 1976; Weeks et al., 1977, 1978). Mellor (1982) was the first to make a field survey of the bathymetry of a few lakes on the North Slope, and to make occasional ice thickness measurements during the winter in conjunction with airborne SAR overflights. In so doing, he was able to show that the temporal and spatial changes of SAR backscatter signatures from the lakes during the course of the winter were closely related to the bathymetry and its effects on ice growth and grounding on the bottom. The SAR and numerical ice growth modelling technique that we have described could be used to map accurately the bathymetry of those lakes that are shallower than the maximum ice thickness, without the need to visit the lakes, except perhaps for validation purposes at a few locations. More accurate mapping would result from more frequent acquisition of SAR data with higher spatial resolution, e.g., ASF ERS-1/ERS-2 Full Resolution products with a pixel size of 12.5 m and spatial resolution of 30 m, or RADARSAT Fine Beam products with a pixel size of 6.25 m and spatial resolution of 10 m (Bicknell and Cuddy, 1995).

For those lakes where some part of the ice cover does not freeze completely each winter, our method determines the depth of the remaining water as being greater than the maximum ice thickness. The bathymetry of these lakes could be mapped accurately to the depth equivalent to the maximum ice thickness. Beyond that, in the case of winter 1991–92, the water depth would simply be noted as greater than 2.2 m. The bathymetric mapping might be improved by further analysis of the tonal variations of the ice cover. Mellor (1982, 1994) has shown that there are subtle SAR image grey scale variations in ice on water that is up to 4 m deep caused by the reduction in the density of tubular bubbles in the ice and the resultant reduction in backscatter. Some of these grey scale variations are evident in the Siberian lakes (e.g., Lakes V and VI, Fig. 7). More detailed mapping of the tonal variations of ice that has liquid water below it at the end of winter might yield information on how much lake water is between the depth of maximum ice thickness and 4 m deep, and how much is more than 4 m deep. Ice on very deep lakes has a uniformly dark tone; the ice is essentially inclusion-free, since deep water provides a large reservoir that does not become supersaturated with the gases rejected during ice growth (Morris et al., 1995). Thus, the combined SAR and numerical modelling technique for lake depth determination is best applied to shallow lakes, where a large portion of the water body is not more than 4 m deep.

ACKNOWLEDGEMENTS

This work was supported by NASA Polar Program Grant NAG 5–1731, Dr. R.H. Thomas, Program Manager. Dorothy Hall, Willy Weeks, and Jack Mellor have been a source of inspiration and encouragement. Stephanie Cushing assisted with the preparation of Figures 4, 5, and 6. The ERS–1 SAR scenes' copyright rests with ESA.

REFERENCES

BENSON, C.S. 1982. Reassessment of winter precipitation on Alaska's Arctic Slope and measurements on the flux of wind blown snow. Geophysical Institute, University of Alaska Report UAG R-288 (September 1982). 26 p.

BICKNELL, T., and CUDDY, D. 1995. Alaska SAR Facility Product Specification. Pasadena, California: NASA, Jet Propulsion Laboratory.

CARSON, C.E., and HUSSEY, K.M. 1962. The oriented lakes of arctic Alaska. Journal of Geology 70(4):417–439.

ELACHI, C., BRYAN, M.L., and WEEKS, W.F. 1976. Imaging radar observations of frozen Arctic lakes. Remote Sensing of Environment 5:169–175.

JEFFRIES, M.O., MORRIS, K., WEEKS, W.F., and WAKABAYASHI, H. 1994. Structural and stratigraphic features and ERS–1 synthetic aperture radar backscatter characteristics of ice growing on shallow lakes in N.W. Alaska, winter 1991–1992. Journal of Geophysical Research 99(C11):22 459–22 471.

LISTON, G.E., and HALL, D.K. 1995a. An energy balance model of lake-ice evolution. Journal of Glaciology 41(138):373–382.

LISTON, G.E., and HALL, D.K. 1995b. Sensitivity of lake freeze-up and break-up to climate change: A physically based modeling study. Annals of Glaciology 21:387–393.

MELLOR, J. 1982. Bathymetry of Alaskan Arctic lakes: A key to resource inventory with remote sensing methods. Ph.D. Thesis, Institute of Marine Science, University of Alaska.

———. 1994. ERS-1 SAR use to determine lake depths in Arctic and sub-Arctic regions. In: Proceedings of the Second ERS-1 Symposium—Space at the Service of our Environment, 11–14 October 1993, Hamburg, Germany, Special Publication SP-361. Paris: European Space Agency. 1141–1146.

MORRIS, K., JEFFRIES, M.O., and WEEKS, W.F. 1995. Ice processes and growth history on Arctic and sub-Arctic lakes using ERS-1 SAR data. Polar Record 31(177):115–128.

SELLMANN, P.V., BROWN, J., LEWELEN, R.I., McKIM, H., and MERRY, C. 1975a. The classification and geomorphic implications of thaw lakes on the Arctic Coastal Plain, Alaska. Special Report No. 344. Hanover, New Hampshire: Cold Regions Research and Engineering Laboratory.

SELLMANN, P.V., WEEKS, W.F., and CAMPBELL, W.J. 1975b. Use of side-looking airborne radar to determine lake depth on

the Alaskan North Slope. Special Report No. 230. Hanover, New Hampshire: Cold Regions Research and Engineering Laboratory.

WAKABAYASHI, H., JEFFRIES, M.O., and WEEKS, W.F. 1994. C band backscatter variation and modelling for lake ice in northern Alaska (in Japanese with English abstract). Journal of the Japanese Remote Sensing Society 14(3):18–27.

WEEKS, W.F., SELLMANN, P.V., and CAMPBELL, W.J. 1977. Interesting features of radar imagery of ice-covered North Slope lakes. Journal of Glaciology 18 (78):129–136.

WEEKS, W.F., FOUNTAIN, A.G., BRYAN, M.L., and ELACHI, C. 1978. Differences in radar returns from ice-covered North Slope lakes. Journal of Geophysical Research 83 (C8):4069–4073.

WEEKS, W.F., GOW, A.J., and SCHERTLER, R.J. 1981. Ground-truth observations of ice-covered North Slope lakes imaged by radar. Research Report 81-19. Hanover, New Hampshire: Cold Regions Research and Engineering Laboratory.